Automated Corpus Callosum Extraction via Laplace-Beltrami Nodal Parcellation and Intrinsic Geodesic Curvature Flows on Surfaces

Rongjie Lai
Department of Mathematics
University of Southerm California
rongjiel@usc.edu

Yonggang Shi
Department of Neurology
University of California, Los Angeles
yshi@loni.ucla.edu

Nancy Sicotte
Cedar Sinai Medical Center
Los Angeles, U. S. A.
nsicotte@ucla.edu

Arthur W. Toga
Department of Neurology
University of California, Los Angeles
arthur.toga@loni.ucla.edu

Abstract

Corpus callosum (CC) is an important structure in human brain anatomy. In this work, we propose a fully automated and robust approach to extract corpus callosum from T1-weighted structural MR images. Our method is composed of two key steps. In the first step, we find an initial guess for the curve representation of CC by using the zero level set of the first nontrivial Laplace-Beltrami (LB) eigenfunction on the white matter surface. In the second step, the initial curve is deformed toward the final solution with a geodesic curvature flow on the white matter surface. For numerical solution of the geodesic curvature flow on surfaces, we represent the contour implicitly on a triangular mesh and develop efficient numerical schemes based on finite element method. Because our method depends only on the intrinsic geometry of the white matter surface, it is robust to orientation differences of the brain across population. In our experiments, we validate the proposed algorithm on 32 brains from a clinical study of multiple sclerosis disease and demonstrate that the accuracy of our results.

1. Introduction

The corpus callosum (CC) is a wide, flat bundle connecting the left and right cerebral hemispheres, and plays an important role in communication between the two hemispheres. Various neuroimaging studies indicate that the size, thickness and shape of CC are related to brain dysfunction [1, 2], gender [3], as well as intelligence [4, 5]. Manual delineation is typically used in clinical and neuroscience research practice. With the increasing availability of large scale data set from multi-site studies for diseases such as Alzheimer's disease, multiple sclerosis, and autism, there is an urgent need for fully automated methods for brain structure segmentation from magnetic resonance (MR) images. In this paper, we propose a novel method for the extraction of the CC using Laplace-Beltrami eigenfunctions and geodesic curvature flows on surfaces. Our method is intrinsic and thus robust to size and orientation variations of brains.

Manually delineating the boundary of CC in the midsagittal slice of an MR image is the most common approach in practice [3], but it is time consuming, highly dependent on researchers' experience, and difficult to reproduce. Based on the midsagittal slice of MR images, various methods for general medical image segmentation [6, 7] have been applied to CC extraction [8, 9, 10]. However, these methods typically require prior knowledge from training data or good initialization from user interactions. In addition, both the manual and semi-automated methods work on the midsagittal slice, which makes them depend on the preprocessing steps used to extract this specific slice.

In this work, we propose a novel and fully automated CC extraction method based on the intrinsic geometry of 3D white matter surfaces. Using the first nontrivial Laplace-Beltrami (LB) eigenfunction, we explicitly capture the symmetry of the white matter surface and obtain an initial curve almost close to the final solution. To further optimize the result, we develop an implicit formulation of geodesic curvature flows on surfaces and use it to minimize the length of the initial curve and compute the final solution. For numerical computation, we work directly on triangulated surfaces by finite element method to realize implicit geodesic curvature flows. In experiments, we demonstrate the geodesic curvature flow in our method and apply it to brains from a clinical study of multiple sclerosis. Comparisons with tissue maps show that our method can automatically generate accurate curve representations of the CC.

The rest of the paper is organized as follows. In Section 2, we briefly review mathematical background of LB eigenfunctions and use the first LB nodal curves to construct an initial curve representation of CC. After that, an implicit formulation of the geodesic curvature flow on surface is introduced to deform the initial guess to the final curve representation of CC in Section 3. Experimental results are presented in Section 4 to demonstrate the performance of our method. Finally, conclusions and future work are discussed in Section 5.

2. Laplace-Beltrami Nodal Curves

Let $(\mathcal{M}, g)$ denote a closed Riemannian surface. For any smooth function $\psi \in C^\infty(\mathcal{M})$, the Laplace-Beltrami (LB) operator is defined as:

$$\triangle_{\mathcal{M}}\psi = \mathrm{div}_{\mathcal{M}}(\nabla_{\mathcal{M}}\psi) = \frac{1}{\sqrt{G}}\sum_{i=1}^{2}\frac{\partial}{\partial x_i}(\sqrt{G}\sum_{j=1}^{2}g^{ij}\frac{\partial \psi}{\partial x_j}) \tag{1}$$

where $\nabla_{\mathcal{M}}$ and $\mathrm{div}_{\mathcal{M}}$ are the surface gradient operator and divergent operator, respectively, (g^{ij}) is the inverse matrix of $g = (g_{ij})$, and $G = \det(g_{ij})$.

The LB operator is self-adjoint and elliptic, so its spectrum is discrete and can be described as follows [11]:

$$\triangle_{\mathcal{M}}\psi_n = -\lambda_n\psi_n,\ n = 0, 1, 2, \cdots. \tag{2}$$

The eigenvalues of $\triangle_{\mathcal{M}}$ can be ordered as $0 = \lambda_0 < \lambda_1 \leqslant \lambda_2 \leqslant \cdots$ and the corresponding eigenfunctions are $\phi_0, \psi_1, \psi_2, \cdots$. Here, $\lambda_0 = 0$ and the corresponding eigenfunction ψ_0 is a constant function on $\mathcal{M}$. Among the rest eigenfunctions, we are particularly interested in the first nontrivial eigenfunction ψ_1, which satisfies the following property:

$$\begin{aligned}\psi_1 &= \arg\min_{\psi\perp\psi_0, ||\psi||=1}\int_{\mathcal{M}}|\nabla_{\mathcal{M}}\psi|^2 \mathrm{d}\mathcal{M},\\ \lambda_1 &= \int_{\mathcal{M}}|\nabla_{\mathcal{M}}\psi_1|^2\mathrm{d}\mathcal{M}.\end{aligned} \tag{3}$$

Numerically, we use the finite element method (FEM) to compute the eigen-system of the LB operator [12, 13]. For any given surface $\mathcal{M}$ in $\mathbb{R}^3$, we represent $\mathcal{M}$ as a triangular mesh $\{V = \{v_i\}_{i=1}^N, T = \{T_l\}_{l=1}^L\}$, where $v_i \in \mathbb{R}^3$ is the i-th vertex and T_l is the l-th triangle. One can choose linear elements $\{e_i\}_{i=1}^N$, which satisfies $e_i(v_j) = \delta_{i,j}$ as the notation of the Kronecker delta symbol, and write $\mathbb{E} = Span_{\mathbb{R}}\{e_i\}_{i=1}^N$. Then the discrete version of the weak formula of the continuous variational problem (2) is to find a $\psi \in \mathbb{E}$ such that

$$\sum_l \int_{T_l}\nabla_{\mathcal{M}}\psi\nabla_{\mathcal{M}}\eta = \lambda\sum_l\int_{T_l}\psi\eta,\ \forall\eta\in\mathbb{E}. \tag{4}$$

If we write

$$\begin{cases}\psi = \sum_i^N x_i e_i\\ A = (a_{ij})_{N\times N}, \quad a_{ij} = \sum_l\int_{T_l}\nabla_{\mathcal{M}}e_i\nabla_{\mathcal{M}}e_j\\ B = (b_{ij})_{N\times N}, \quad b_{ij} = \sum_l\int_{T_l}e_ie_j,\end{cases} \tag{5}$$

where the stiffness matrix A is symmetric and the mass matrix B is symmetric and positive definite, the discrete variational problem is equivalent to the generalized matrix eigenproblem:

$$\begin{cases}Ax = \lambda Bx, \text{where } x = (x_1, \cdots, x_N)^T\\ \psi = \sum_i^N x_i e_i.\end{cases} \tag{6}$$

Note that both A and B are $N \times N$ sparse matrices. There are a variety of numerical packages to solve the above problem. For instance, this can be solved with existing numerical packages in MATLAB. In Figure 1 (a), we show a computation result for the first nontrivial eigenfunction on a white matter surface.

Due to the intrinsic nature of the LB operator and its eigenfunctions, ψ_1 has the following remarkable properties [14, 11]:

1. ψ_1 is intrinsic and isometric invariant. Thus properties derived from ψ_1 are robust to rigid translation and pose variations.

2. Let $\Gamma^0 = \{p \in \mathcal{M} \mid \psi_1(p) = 0\}$ be the zero-th level curve of ψ_1, which is so called **the first LB nodal curve** (See Fig.1). Cheng [14] proved that Γ^0 forms continuous curves on $\mathcal{M}$. In addition, Γ divides $\mathcal{M}$ into two connected components.

The above properties ensure that the first LB nodal curves define a set of well-behaved curves on the given surface, and they are robust to surface pose variations. Moreover, Ulenbeck proves that ψ_1 is a Morse function for general surfaces [15]. Thus, ψ_1 can be used to detect surface global structures such as symmetry. In practice, Shi et al. [16, 17] proposed to utilize ψ_1 to model the global shape of elongated structures. In addition, due to the energy formula of ψ_1 in (3), we can observe that ψ_1 only depends on how $\nabla_{\mathcal{M}}$ distribute on surfaces, which is further related to surface local geometry. For the CC extraction problem, the target surface is the white matter surface, which has a symmetric structure between the left and right hemispheres. This symmetry will guide the position of the zeroth level curve of ψ_1 to appear in the middle of the two hemispheres on the white matter surface. Therefore, the zeroth level curve of the first nontrivial eigenfunction ψ_1 provides a very good

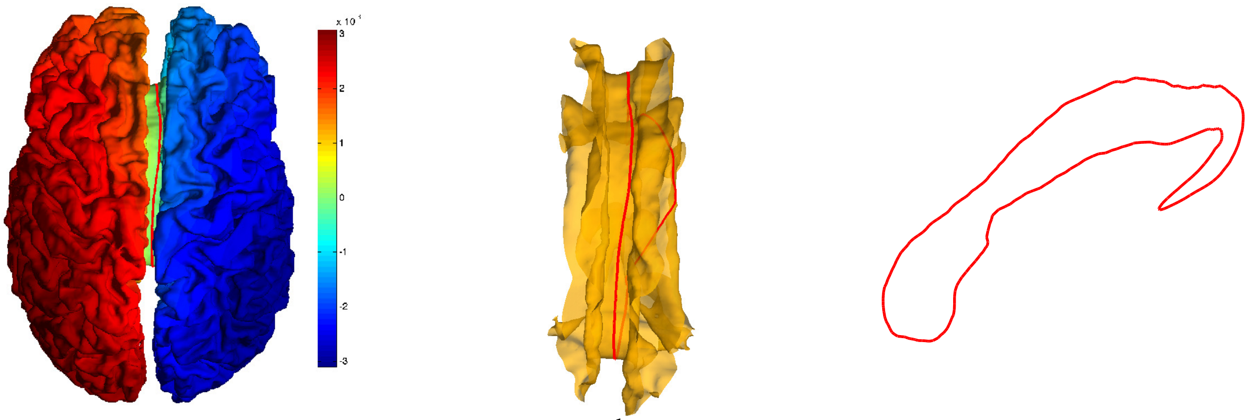

a b c

Figure 1. (a) The surface is color coded by the first nontrivial LB eigenfunction ψ_1 and the red contour marks the zero level set of ψ_1. (b) A zoom-in of (a) around the middle part of the white matter surface. (c) The zeroth level curve Γ^0 of ψ_1.

initial guess of the curve representation of CC as illustrated in Fig.1 (b) and (c).

However, there are limitations in this initial guess of the CC. In Fig.1 (b), it is clear to observe that the initial curve is not a satisfactory representation of the CC because it does not exactly sit on the middle of the left and right cerebral hemispheres. This is because the left and right hemispheres are not completely symmetric. Intuitively speaking, this initial curve is not "straight"on the middle part of white matter surface. Mathematically, we require that the curve representation Γ of CC should be a geodesic curve between the left and right cerebral hemispheres so that it can correctly separate the two cerebral hemispheres. This condition is not always satisfied for the initial guess constructed from the first LB nodal curve, since the position of the LB nodal curve depends on the degree of symmetry between the left and right cerebral hemispheres. To tackle this problem, we propose to utilize geodesic curvature evolution to optimize the initial curve in the following section.

3. Geodesic Curve Evolutions on Surfaces

In this section, we develop a variational model for curve evolution on surfaces. By minimizing a curve length energy on surfaces, we deform the initial curve obtained in Section. 2 and compute a geodesic solution for CC segmentation.

3.1. Geodesic curvature flows

Given a surface $\mathcal{M} \subset \mathbb{R}^3$ and a unit speed surface curve $\Gamma : [0, L] \to \mathcal{M}$, we consider the following energy E_c related to geodesic curvature flow to obtain geodesics on the surface $\mathcal{M}$:

$$E_c(\Gamma) = \int_\Gamma \mathrm{d}s. \tag{7}$$

By minimizing this energy, we can deform the initial curve Γ^0 obtained in section 2 on $\mathcal{M}$ in the gradient de-

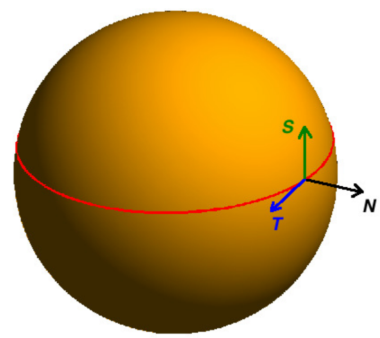

Figure 2. The red contour represents a curve Γ on surface $\mathcal{M}$. $\vec{S}$ is the intrinsic normal, $\vec{T}$ is the tangent vector and $\vec{N}$ is the normal vector of $\mathcal{M}$.

scent direction. Namely, the desired curve deformation can be described as follows:

$$\begin{cases} \frac{\mathrm{d}\Gamma}{\mathrm{d}t} = \kappa_g \vec{S} \\ \Gamma(0) = \Gamma_0 = \psi_1^{-1}(0) \end{cases} \tag{8}$$

Here, $\vec{S}$ is the intrinsic normal of Γ in $\mathcal{M}$ and $\kappa_g = \langle \Gamma'', \vec{S} \rangle$ is the geodesic curvature of Γ, which measures how Γ is curved on the surface $\mathcal{M}$. It is easy to observe that the curve in steady state of the flow in (8) satisfies $\kappa_g = 0$ and is a geodesic curve on $\mathcal{M}$. This geodesic curvature flow on a 3D surface is a generalization of geodesic active contours in 2D Euclidean planes [18, 19]. The behavior of geodesic curvature flows on surfaces, however, are much more complicated than geodesic active contours on Euclidean planes because the surface geometry will also affect the curve evolution [20, 21, 22]. More recently, a level set formulation of geodesic curvature flow on surfaces was discussed in [23, 24, 25].

Similar to implicit formulations for curve evolution in Euclidean spaces [26], we consider implicit representation of the geodesic curvature flow $\Gamma(t)$ on the closed surface $\mathcal{M}$ by a functional flow $\phi : \mathcal{M} \times [0, \infty) \to \mathbb{R}$. Namely, we represent each curve as $\Gamma(t) = \phi^{-1}(0, t)$. Therefore

$$\begin{aligned} \phi(\Gamma(t), t) &= 0 \\ \Longrightarrow \quad \nabla_{\mathcal{M}}\phi \cdot \frac{\mathrm{d}\Gamma}{\mathrm{d}t} &+ \phi_t = 0 \end{aligned} \tag{9}$$

Moreover, Γ's geodesic curvature κ_g can be given by $\mathrm{div}_{\mathcal{M}}(\frac{\nabla_{\mathcal{M}}\phi}{|\nabla_{\mathcal{M}}\phi|})|_{\Gamma}$ [27], and the intrinsic normal direction $\vec{S}$ of Γ can be given by $\vec{S} = -\frac{\nabla_{\mathcal{M}}\phi}{|\nabla_{\mathcal{M}}\phi|}$. Thus, by combining equations (8) and (9), we can write down the implicit representation of the geodesic curvature flow in (8) as follows:

$$\begin{cases} \phi_t = |\nabla_{\mathcal{M}}\phi| \mathrm{div}_{\mathcal{M}}\left(\frac{\nabla_{\mathcal{M}}\phi}{|\nabla_{\mathcal{M}}\phi|}\right) \\ \phi(0) = \text{the signed distance function of } \Gamma_0 \text{ on } \mathcal{M} \end{cases} \tag{10}$$

where the signed distance function of Γ^0 on $\mathcal{M}$ can be computed with the fast marching method on triangulated surface $\mathcal{M}$ [28]. From the variational point of view, the corresponding implicit formulation of the energy function E_c is:

$$E_c(\phi) = \int_{\phi^{-1}(0)} \mathrm{d}s = \int_{\mathcal{M}} \delta(\phi)|\nabla_{\mathcal{M}}\phi| \mathrm{d}\mathcal{M} \tag{11}$$

where abuse of notation, $\phi : \mathcal{M} \to \mathbb{R}$, is using for a implicit representation of a curve on $\mathcal{M}$, and $\delta(\cdot)$ is the standard Delta function. Then, (10) is the gradient flow of (11). Note the above development assumes the surface $\mathcal{M}$ is closed and has no boundary. In the case $\mathcal{M}$ is an open surface with boundary $\partial\mathcal{M}$, the corresponding implicit representation of the geodesic curvature flow on $\mathcal{M}$ can be expressed as:

$$\begin{cases} \phi_t = |\nabla_{\mathcal{M}}\phi| \mathrm{div}_{\mathcal{M}}\left(\frac{\nabla_{\mathcal{M}}\phi}{|\nabla_{\mathcal{M}}\phi|}\right) \\ \phi(0) = \text{the signed distance function of } \Gamma_0 \text{ on } \mathcal{M} \\ \frac{\partial\phi}{\partial\vec{n}} = 0, \text{ on } \partial\mathcal{M} \end{cases} \tag{12}$$

where $\vec{n}$ is the outward normal of the boundary $\partial\mathcal{M}$.

3.2. Numerical Implementation

To solve the implicit geodesic curvature flow on surfaces, Cheng et al. [23] propose to utilize level set representation of surface $\mathcal{M}$ and approximate the solution of this problem in regular grids. For white matter surfaces with complicated geometry, this method needs highly redundant computation and data storage. More recently, Spira et al. [24] tackle this problem on parametric surfaces, which needs to first solve the challenging problem of parameterizing the white matter surface. Wu et al. [25] propose to use the finite volume method on triangulated surfaces to solve an approximate version of the original problem. In this section, we develop a novel numerical scheme to directly solve this problem on triangulated surfaces based on the finite element method. Our method has very simple formulation, is easy to implement, and computationally efficient because all calculations are on sparse matrices. The numerical schemes developed here is also general and applicable for surfaces with high genus and complicated geometry.

First of all, we write down the implicit geodesic curvature flow (10) as follows:

$$\phi_t = |\nabla_{\mathcal{M}}\phi| \mathrm{div}_{\mathcal{M}}\left(\frac{\nabla_{\mathcal{M}}\phi}{|\nabla_{\mathcal{M}}\phi|}\right) = \triangle_{\mathcal{M}}\phi + g(\phi) \tag{13}$$

where $g(\phi) = -\frac{\nabla_{\mathcal{M}}\phi \cdot \nabla_{\mathcal{M}}(|\nabla_{\mathcal{M}}\phi|)}{|\nabla_{\mathcal{M}}\phi|}$.

To solve the above flow on a triangulated surface $\mathcal{M}$, we consider the semi-implicit Galerkin scheme. Let us denote the standard inner product as $\langle f, g\rangle = \int_{\mathcal{M}} fg\mathrm{d}\mathcal{M}$. For any test function $\eta \in \mathcal{C}^{\infty}(\mathcal{M})$, the weak form of the gradient flow (13) is as follows:

$$\langle \phi_t, \eta\rangle + \langle \nabla_{\mathcal{M}}\phi, \nabla\eta\rangle = \langle g(\phi), \eta\rangle. \tag{14}$$

With the same finite element notation as we discussed in Section 2, the discretization of the above equation can be described as follows:

$$\langle \frac{\phi^n - \phi^{n-1}}{\Delta t}, \eta\rangle + \langle \frac{\nabla_{\mathcal{M}}\phi^n + \nabla_{\mathcal{M}}\phi^{n-1}}{2}, \nabla\eta\rangle = \langle g(\phi^{n-1}), \eta\rangle,$$

Therefore, we need to iteratively solve the following equation:

$$B\phi^n + \frac{1}{2}\Delta t A\phi^n = B\phi^{n-1} - \frac{1}{2}\Delta t A\phi^{n-1} + \Delta t B g(\phi^{n-1})$$

In other words, we need to solve:

$$\phi^n = (B + \frac{1}{2}\Delta t A)^{-1}\Big((B - \frac{1}{2}\Delta t A)\phi^{n-1} + \Delta t B g(\phi^{n-1})\Big)$$

where A is the stiffness matrix and B is the mass matrix defined in (5). Therefore, the numerical scheme of the implicit curve evolution on $\mathcal{M}$ with the initial curve Γ^0 is given as follows:

$$\begin{cases} \phi^n = (B + \frac{1}{2}\Delta t A)^{-1}(B - \frac{1}{2}\Delta t A)\phi^{n-1} \\ \qquad + \Delta t(B + \frac{1}{2}\Delta t A)^{-1} B g(\phi^{n-1}) \\ \phi^0 = \text{signed distance function of } \Gamma^0 = \psi_1^{-1}(0) \text{ on } \mathcal{M}. \end{cases} \tag{15}$$

The above equation shows that we can solve the geodesic curvature flow problem on triangulated meshes with a series of matrix operations. Because the stiffness matrix A and mass matrix B are symmetric and sparse, the above equations can be solved efficiently. At each iteration, the corresponding curve evolution is:

$$\begin{cases} \Gamma^n = (\phi^n)^{-1}(0) \\ \Gamma^0 = (\phi^0)^{-1}(0) = \psi_1^{-1}(0). \end{cases} \tag{16}$$

In summary, the novel approach we develop for CC extraction can be described as follows:

1. Compute the first nontrivial eigenfunction ψ_1 of a given white matter surface, and use the first LB nodal curve $\Gamma^0 = \psi_1^{-1}(0)$ as the initial curve;

2. To find the optimal curve representation of CC, we deform the initial curve Γ^0 using the implicit geodesic curvature flow developed in this section.

In contrast to manual delineation and other segmentation approaches, the method proposed here uses intrinsic geometry to automatically compute the curve representation of CC. Moreover, the proposed method is very robust to the segmentation of white matter surfaces. Since the boundary of CC and other tissues near midsagittal slice are quite clear, the main challenge of white matter segmentation is correct extraction of sulci and gyri regions. However, the first nontrivial LB eigenfunction is very robust to small variations of surface geometry, which leads to the robustness of the initial guess to the small variations due to sulci/gyri segmentation of white matter surfaces. In addition, the results of geodesic curvature flow only depend on the surface geometry near CC regions that usually can be clearly segmented. Overall, the proposed method tackles the problem of of finding midsagittal slices from MR image volumes in previous methods, and it is robust to white matter surface segmentation and pose variations across population.

4. Experimental Results

In this section, experimental results are presented to demonstrate the performance of our method. For all experiments, we first perform tissue classification on each input MR image and automatically extract the white matter surface by applying the fast evolution method in [29] to find the boundary of the white matter region. After that, the method developed in this paper is applied to automatically compute the CC. In the first experiment, we present a detailed analysis of our algorithm on the example used in Section 2. After that, we test our method on 32 images from a clinical study of multiple sclerosis to further illustrate and validate its robustness and accuracy.

4.1. Intrinsic curve evolution process in corpus collasum extraction

As a demonstration of the proposed algorithm, we choose the white matter surface and initial curve Γ^0 shown in Fig. 1. The initial curve Γ^0 is deformed by the geodesic curvature flow for 2500 steps with the time step $\Delta t = 0.5$. In Fig. 3 (a) and (b), we plot the initial curve Γ^0 and the final curve in red and blue color, respectively. It is clear to see that the blue curve is much more straight than the red curve on the surface and serves as a better representation of the CC. In addition, we plot the length of the curve during each iteration of the geodesic curvature flow in Fig. 3 (c), which

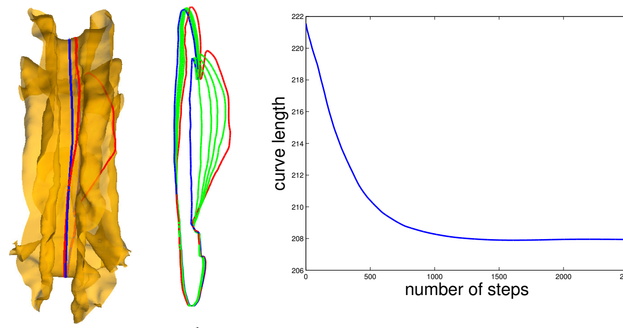

a b c

Figure 3. (a) The red contour marks the initial curve Γ^0 and the blue contour marks the optimal curve deformed by the geodesic curvature flow; (b) The red contour marks the initial curve Γ^0, the green contours mark intermediate curves, and the blue contour marks the optimal curve; (c) Length of intermediate curves in the evolution process.

shows that the geodesic curvature flow minimizes the curve length energy and iteratively deforms the initial curve Γ^0 to a steady state that achieves the shortest length. To compare our result with the MR image, we project the optimal curve onto the midsagittal slice. As shown in Fig. 4, the initial curve does not accurately segment the boundary of the CC because of its inaccurate position on the white matter surface. With the geodesic curvature flow, it is clear to see the improvement from the initial curve to the optimal curve. The two zoom-in images in Fig. 4 (b) and (c) also show the excellent accuracy achieved by our method in CC extraction.

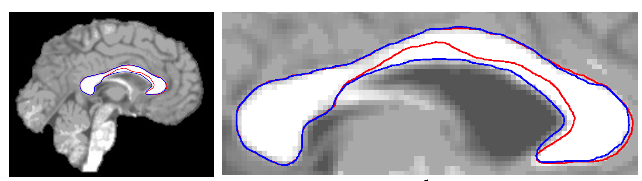
a b

Figure 4. The red contour marks the initial curve Γ^0 and the blue contour marks the optimal curve deformed by geodesic curvature flow. (b) is the amplificatory images of (a).

4.2. Validation on a clinical data set

In this section, we further validate the robustness and accuracy of the proposed method by testing it on 32 MR images from a clinical data set for multiple sclerosis study. In our experiments, the CC on all images are computed successfully with the geodesic curvature flow in about 2000 steps with the time step $\Delta t = 0.5$. In Fig. 5, we plot 32 pairs of length comparisons between the initial curves obtained by the first LB nodal curves and the optimal curves obtained by the geodesic curvature flow. In Fig. 6, we plot the seg-

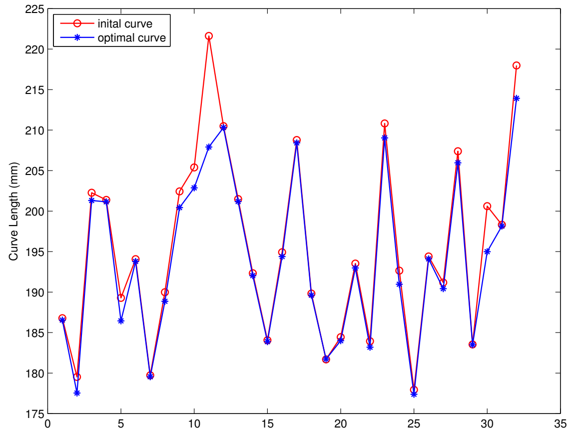

Figure 5. Length comparisons between the initial curves (IC) and optimal curves (OC). Initial curves are marked as red circles and the corresponding optimal curves are marked as blue stars.

mentation results on the midsagittal slice of corresponding MR images near CC regions. As the theoretical expectation of geodesics, the optimal curves obtained by geodesic curvature flow do optimize the initial guess and contribute more robustness and accurate results as we illustrated in Fig. 6. While the initial guess curves obtained from the first nontrivial LB eigenfunctions usually give fairly good approximations, we can see the geodesic curvature flow can provide significant improvement even when the initial guess is quite tilted due to asymmetry in the white matter surface. The combination of these steps ensures the robustness and accuracy of the overall approach.

5. Conclusion and Future Work

In this paper, we proposed a novel method to extract the curve representation of CC from automatically generated white matter surfaces. Our approach can be realized in two steps. In the first step, we compute the first nontrivial LB eigenfunction of the given white matter surface and use its zeroth level curve as the initial guess. In the second step, we deform the initial guess using the geodesic curvature flow on the white matter surface to optimize the curve representation. Our method is completely determined by the intrinsic geometry of the white matter surface. Therefore, it provides an automated and robust approach for the construction of the curve representation of CC. In future work, we will perform validations on large data sets and apply it to studies of callosal morphology in pathology and normal development.

Acknowledgments

Rongjie Lai' s work was supported by the USC Zumberge Individual Award. This work was also supported by NIH 5P41RR013642 and DoD W81XWH-10-1-0882.

References

[1] J. Duncan, A. Wang, A. Amini, R. Greene, L. Kier, J. Gore, J. Holahan, S. Shaywitz, J. Fletcher, R. Bronen, and B. Shaywitz. A mri-based study of the corpus callosum in dyslexic and normal children. *Neurology*, 1996. 1

[2] M. Frumin and P. Golland et al. Shape differences in the corpus callosum in first psychotic episode schizophrenia and first psychotic episode affective disorder. *American Journal of Psychiatry*, 159::866–868, 2002. 1

[3] E. Luders, K. L. Narr, E. Zaidel, P. Thompson, and A. W. Toga. Gender effects on callosal thickness in scaled and unscaled space. *NeuroReport*, 17(11):1103–1106, 2006. 1

[4] C. Davatzikos, A. Barzi, T. Lawrie, A. H. Hoon Jr., and E. R. Melhem. Correlation of corpus callosal morphometry with cognitive and motor function in periventricular leukomalacia. *Neuropediatrics*, 34:247–251, 2003. 1

[5] E. Luders, K. L. Narr, R. M. Bilder, P. Thompson, P. R. Szeszko, L. Hamilton, and A. W. Toga. Positive correlations between corpus callosum thickness and intelligence. *Neuroimage*, 37(4):1457–64, 2007. 1

[6] T. Cootes, C. Taylor, D. Cooper, and J. Graham. Active shape models -their training and application. *Computer Vision and Image Understanding*, 61(1):38–59, 1995. 1

[7] T. McInerney, G. Hamarneh, M. Shenton, and D. Terzopoulos. Deformable organisms for automatic medical image analysis. *Medical Image Analysis*, 6(3):251—266, 2002. 1

[8] A. Lundervold, N. Duta, T. Taxt, and A. K. Jain. Model-guided segmentation of corpus callosum in MR images. *CVPR*, 1999. 1

[9] M. Taron, N. Paragios, and M-P. Jolly. Uncertainty-driven non-parametric knowledge-based segmentation: The corpus callosum case. *IEEE (ICCV) Workshop on VLSM*, 2005. 1

[10] Q. He, Y. Duan, J. Miles, and N. Takahashi. A context-sensitive active contour for 2d corpus callosum segmentation. *International Journal of Biomedial Imaging*, 2007. 1

[11] D. Jankobson, N. Nadirashbili, and J. Toth. Geometric propertiess of eigenfunctions. *Russian Math. Surveys*, 56(6):1085–1105, 2001. 2

[12] M. Reuter, F.E. Wolter, and N. Peinecke. Laplace-Beltrami spectra as Shape-DNA of surfaces and solids. *Computer-Aided Design*, 38:342–366, 2006. 2

[13] A. Qiu, D. Bitouk, and M. I. Miller. Smooth functional and structural maps on the neocortex via orthonormal bases of the Laplace-Beltrami operator. *IEEE Trans. Med. Imag.*, 25(10):1296–1306, 2006. 2

[14] S.-Y. Cheng. Eigenfunctions and nodal sets. *Comment. Math. Helvetici*, 51:43–55, 1976. 2

[15] K. Uhlenbeck. Generic properties of eigenfunctions. *Amer. J. of Math.*, 98(4):1059–1078, 1976. 2

[16] Y. Shi, R. Lai, S. Krishna, N. Sicotte, I. Dinov, and A. W. Toga. Anisotropic Laplace-Beltrami eigenmaps: Bridging Reeb graphs and skeletons. In *Proc. MMBIA*, 2008. 2

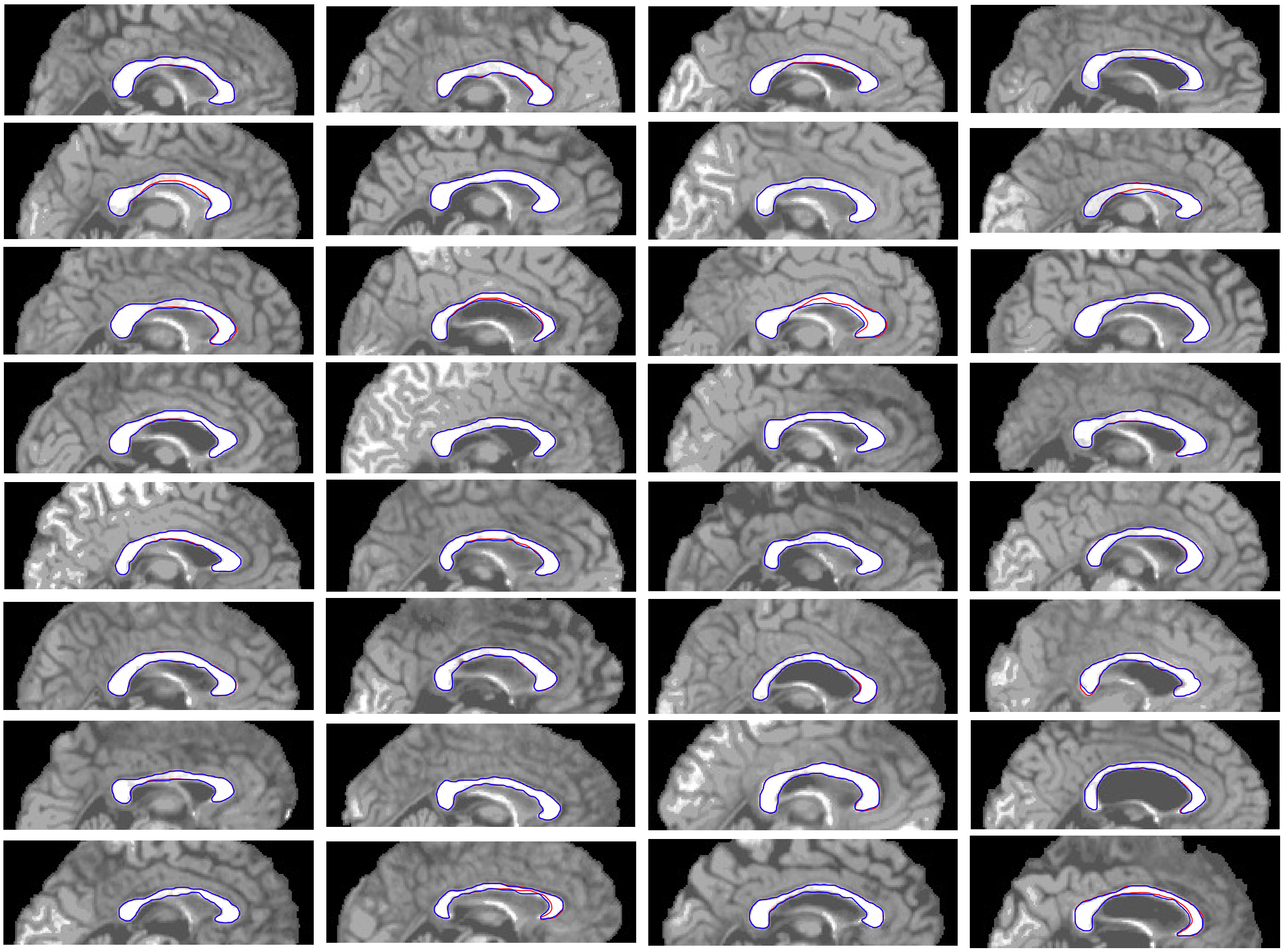

Figure 6. The red contours mark the initial curves and the blue contours mark the optimal curves deformed by geodesic curvature flows.

[17] Y. Shi, J. H. Morra, P. Thompson, and A. W. Toga. Inverse-consistent surface mapping with inverse-consistent surface mapping with laplace-beltrami eigen-features. *IPMI*, 2009. 2

[18] M. Kass, A. Witkin, and D. Terzopoulos. Snakes:active contour models. *International Journal of Computer Vision*, 1988. 3

[19] V. Caselles, R. Kimmel, and G. Sapiro. Geodesic active coutours. *Proc. 5th Int. Conf. Computer Vision*, pages 694–699, 1995. 3

[20] R. S. Millman and G. D. Parker. *Elements of Differential Geometry*. Prentice-Hall, 1977. 3

[21] M. Gage. Curve shortening on surfaces. *Ann. Sci. Ecol Norm. Sup.*, 23(2):229–256, 1990. 3

[22] K. Mikula and D. Sevcovic. Evolution of curves on a surface driven by the geodesic curvature and external force. *Applicable Analysis.*, 85(4):345–362, 2006. 3

[23] L.-T. Cheng, P. Burchard, B. Merriman, and S. Osher. Motion of curves constrained on surfaces using a level-set approach. *J. Comput. Phys.*, 175(2):604–644, 2002. 3, 4

[24] A. Spira and R. Kimmel. Geometric curve flows on parametric manifolds. *J. Comp. Phys.*, 223(235–249), 2007. 3, 4

[25] C. Wu and X. Tai. A level set formulation of geodesic curvature flow on simplicial surfaces. *IEEE Transactions on Visualization and Computer Graphics*, 2010. 3, 4

[26] S. Osher and J. Sethian. Fronts propagation with curvature-dependent speed: algorithms based on Hamilton-Jacobi formulations. *Journal of computational physics*, 79(1):12–49, 1988. 3

[27] L. M. Lui. *Computational Conformal Geometry and Its Applications to Human Brain Mapping*. PhD thesis, UCLA, July 2008. 4

[28] R. Kimmel and J. A. Sethian. Computing geodesic paths on manifolds. *Proc. Natl. Acad. Sci. USA*, 95(15):8431–8435, 1998. 4

[29] Y. Shi, R. Lai, J. Morra, I. Dinov, P. Thompson, and A. W. Toga. Robust surface reconstruction via laplace-beltrami eigen-projection and boundary deformation. *IEEE Trans. Medical Imaging*, 29(12):2009–2022, 2010. 5